

Discovery of $H\alpha$ satellite emission in a low state of the SW Sextantis star BB Doradus ^{*}

L. Schmidtbreick^{1†}, P. Rodríguez-Gil^{2,3,4}, K. S. Long⁵, B. T. Gänsicke⁶,
C. Tappert⁷, M. A. P. Torres^{8,9}

¹*European Southern Observatory, Casilla 19001, Santiago 19, Chile*

²*Instituto de Astrofísica de Canarias, Vía Láctea s/n, La Laguna, E-38205, Santa Cruz de Tenerife, Spain*

³*Departamento de Astrofísica, Universidad de La Laguna, La Laguna, E-38203, Santa Cruz de Tenerife, Spain*

⁴*Isaac Newton Group of Telescopes, Apartado de correos 321, E-38700 Santa Cruz de la Palma, Spain*

⁵*Space Telescope Science Institute, 3700 San Martin Drive, Baltimore, MD 21218, USA*

⁶*Department of Physics, University of Warwick, Coventry CV4 7AL, UK*

⁷*Departamento de Física y Astronomía, Universidad de Valparaíso, Avda. Gran Bretaña 1111, Valparaíso, Chile*

⁸*SRON, Netherlands Institute for Space Research, Sorbonnelaan 2, 3584 CA, Utrecht, The Netherlands*

⁹*Harvard-Smithsonian Center for Astrophysics, 60 Garden Street, Cambridge, MA 02138, USA*

XXXX

ABSTRACT

BB Dor was observed during its low state state in 2009. Signatures of both binary components are revealed in the average optical spectrum; no signature of accretion is observed. Narrow emission lines of $H\alpha$, He I and Na-D, as well as TiO absorption troughs trace the motion of the irradiated secondary star. We detect two additional components in the $H\alpha$ emission line that share many characteristics of similar "satellite" lines observed in the low state of magnetic cataclysmic variables of AM Her type. It is the first time such emission components are detected for an SW Sex star.

Key words: Physical data and processes: accretion, accretion discs stars: activity – fundamental parameters – novae, cataclysmic variables – individual:BB Dor – magnetic fields – winds, outflows

1 INTRODUCTION

BB Doradus is a cataclysmic variable (CV) of the SW Sextantis type. With typical periods between 3 h and 4 h these stars populate the upper edge of the period gap and are believed to experience very high mass transfer rates. For a summary on this subgroup, see the original paper by Thorstensen et al. (1991) and a more recent review by Rodríguez-Gil et al. (2007). Some of these stars show occasional low states when mass transfer is reduced or even completely suppressed resulting in a brightness drop by $\sim 3 - 5$ mag. The stars can stay at these low level for weeks or months before rising again to their "normal" high state. The advantage in observing the binary at low state lies in the reduced mass transfer which thus results in a weak or absent accretion disc. While the disc usually dominates the emission of a high mass transfer CV, in low state one has a chance to observe signatures of the binary components: the white dwarf primary and the secondary star. To our knowledge, the individual binary components could

be observed for only three systems in such a low state: DW UMa (Araujo-Betancor et al. 2003; Knigge et al. 2004), TT Ari (Gänsicke et al. 1999), and MV Lyr (Hoard et al. 2004). In the context of an ongoing large program to study SW Sextantis stars (see e.g. Rodríguez-Gil et al. (2007)), we monitor several of them photometrically to register when they enter one of these rare low states and thus trigger detailed observations during this phase. For more information on this project, see Rodríguez-Gil et al. (2011).

2 OBSERVATIONS AND DATA REDUCTION

Time-resolved spectroscopic data were obtained on 2009 Jan 17 between 00:30 and 07:00 UT when BB Dor was well in a low state that lasted from May 2008 to April 2009 (Rodríguez-Gil et al. 2012). Target-of-Opportunity observations were triggered for the FOCAL Reducer and low dispersion Spectrograph (FORS2) (Appenzeller et al. 1998) on the Very Large Telescope (VLT) on Paranal, operated by the European Southern Observatory (ESO). We opted for GRIS1200R+93 and a $0.7''$ slit to concentrate on the $H\alpha$ emission line. Clear skies and a stable seeing around $0.8''$ allowed to observe 65 spectra with an individual exposure

^{*} Based on observations collected at the European Southern Observatory, Paranal (program 082.D-0154).

[†] E-mail: lschmidt@eso.org

time of 300 s. In total, we covered 6.5 h, about 1.5 orbital cycles of BB Dor.

The data were reduced using standard procedures in IRAF¹. Further analysis was done using MOLLY², MIDAS³, and self-written C-routines. The spectra were optimally extracted following the method by Horne (1986), the final Full-Width-at-Half-Maximum (FWHM) resolution is 2.05 Å. We used standard star observations to flux-calibrate the spectra. The night was classified as clear but not photometric so thin clouds might have been passing occasionally. Therefore, we do not claim the absolute flux values to be accurate by more than 0.5 mag. However, the flux-calibration removes the detector specific spectral response and yields relative flux values that can be compared within the average spectrum.

3 RESULTS

3.1 The average spectrum

In Fig. 1, the average of the 65 spectra is plotted. It is dominated by narrow emission lines of hydrogen and helium. The FWHM of H α is 6.9 Å, the He I lines have 3.4 Å on average. Rodríguez-Gil et al. (2012) show that accretion events in BB Dor during this low state happen rarely. These epochs can be clearly distinguished from those without accretion as the spectra show broader emission line profiles and a bluer continuum when accretion happens. We compared the line profiles and continuum in the individual spectra with those in Rodríguez-Gil et al. (2012) and find no indication of an accretion event in our data. Indeed, the widths of the lines are narrow and very stable throughout the observations as expected for a non-accreting CV where the origin of such emission lies in the chromosphere or irradiated surface of the companion. This is also confirmed later in this paper by our study of radial velocities.

Around the H α and He I emission lines one can detect weak but broad absorption features. Their origin is most certainly the white dwarf which has been accreting until recently and thus is expected to have He present in its atmosphere. The presence of He I rather than He II suggests a white dwarf temperature between 20000 K and 40000 K which is rather low compared to other SW Sex type stars (MV Lyr: 47000 K, DW UMa: 50000 K, TT Ari: 39000 K, Townsley & Gänsicke 2009). Still, it is in agreement with the value $T = 37000$ K found from Far UV spectroscopy of BB Dor in high state (Godon et al. 2008) and a value between 25000 K and 30000 K found by Rodríguez-Gil et al. (2012) from a WD+M dwarf composite fit to a spectrum covering the whole visual spectral range of BB Dor in quiescence.

We checked the absorption lines for the presence of Zeeman-splitting to get an estimation for a possible magnetic field on the white dwarf. No splitting was detected in

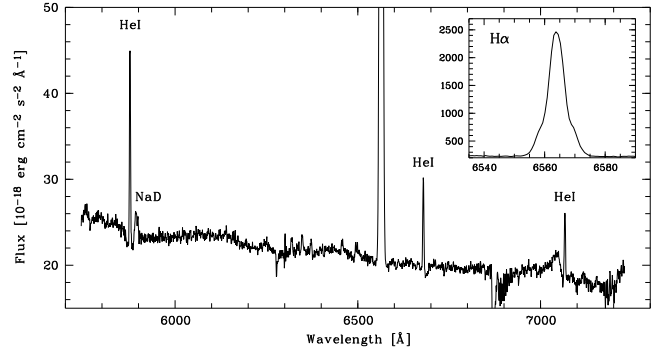


Figure 1. The average of our 65 spectra. The main emission lines are labelled. In the upper right corner a zoom on H α is given.

any of these lines. From this we infer an upper limit of the magnetic field to about 5 MG.

The secondary star shows itself through the presence of weak TiO absorption troughs.

3.2 The H α emission distribution

Radial velocities were measured by fitting Gaussians of 300 km s⁻¹ width to the core of the H α emission lines. Using the analysis-of-variance algorithm (Schwarzenberg-Czerny 1989) as implemented in MIDAS we found the most likely orbital period $P = 0.149(4)$ days. This value is in agreement with Rodríguez-Gil et al. (2012) and places BB Dor right at the centre of the period distribution of the SW Sex stars. By combining their multi-epoch data with our data Rodríguez-Gil et al. derive a much more precise value for the orbital period of $P = 0.154095(3)$ days. We adopt this latter value for all our further analysis, and also use their zero-phase $T_0(\text{HJD}) = 2454833.7779 \pm 0.0003$ defined as the blue-to-red crossing of the H α velocities.

Studying the H α emission line in more detail reveals a remarkable structure: Its line profile consists of at least three components, a central emission line and two satellite lines (see zoom in Fig. 2). Their orbital variation is demonstrated in the plot on the right: the trailed spectra diagram of H α . The two satellite lines can be clearly distinguished. They have the same radial velocity amplitude of 340 km s⁻¹ which is larger than that of the central line. They are symmetrically offset in phase by $\pm 0.15(2)$.

These are the first ever observations of such satellite lines in an SW Sex star. However, such satellite lines were detected before in the quiescent states of polars, i.e. strongly magnetic CVs (Kafka et al. 2005, 2006, 2007, 2008, 2010; Mason et al. 2008). First hints for such an additional emission are also present in earlier low resolution data of AM Her (Latham et al. 1981). We also find indications for a similar feature in the low-state spectra of the non-magnetic nova-like TT Ari that were, however, interpreted differently at the time (Shafter et al. 1985): In their Figure 10, a small line component is visibly moving around the central H α line. The radial velocity of this component is given in their Figure 13. While it is fitted there with a single sinusoid, the data could in retrospect also be interpreted as two crossing sinusoids as we observe them in BB Dor. In the detached binary V471 Tau, Young et al. (1991) observe such additional line components and interpret them as evidence for extended

¹ IRAF is distributed by the National Optical Astronomy Observatories

² Tom Marsh's package MOLLY is available at <http://deneb.astro.warwick.ac.uk/phsaap/software/>

³ MIDAS is distributed by the European Southern Observatory at <http://www.eso.org/sci/software/esomidas/>

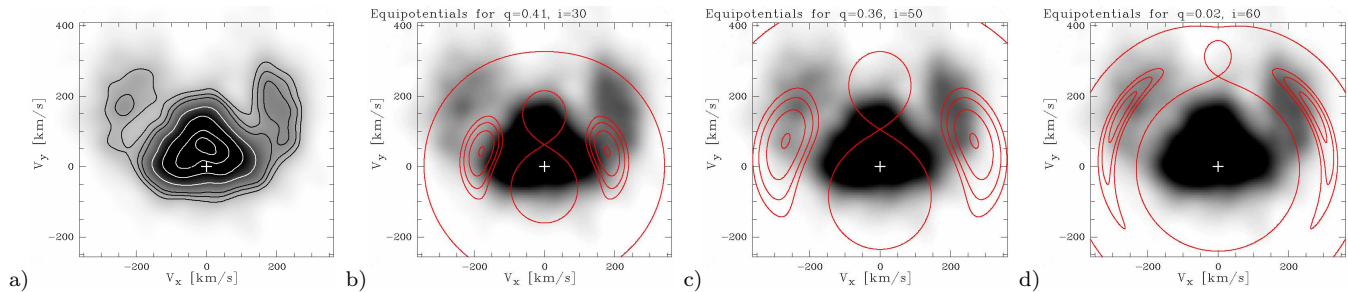


Figure 3. Doppler map of the H α emission distribution in BB Dor. On the left side, the contours of the emission distribution are overlotted. The three images to the right have the Roche equipotentials overplotted for different mass ratios and inclinations, see text for details. The centre of mass is given as +. No match using reasonable parameters can be found between the symmetrical, extended structure and the outer Lagrangian points

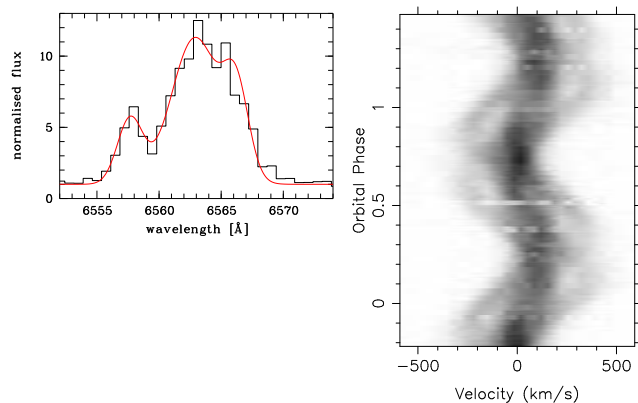


Figure 2. On the left, a zoom on the H α line of an example spectrum (orbital phase 0.93) is plotted with a 3-Gaussian fit for the central line and two satellite lines. The trailed spectra diagram on the right shows the orbital variation of the line profile.

clouds or a ring of plasma orbiting the K-dwarf secondary. All these observations indicate that the here presented feature of satellite lines might be common to a number of CVs and related objects and is not necessarily limited to magnetic ones.

Comparing our data to the well-observed AM Her stars, the appearance of these satellite lines is strikingly similar. Kafka et al. (2008) discuss partial loops of streaming gas co-rotating with the donor star or collimated jet-like outflows as possible origin for these satellite lines. However, the interpretation remains vague due to the uncertainty whether the lines follow crossing or parallel sinusoids. In the case of AM Her, the lines were not sufficiently resolved for this distinction, while the other data are of even poorer quality or do not cover a complete orbit. Only for BL H γ i, Kafka et al. (2010) conclude that crossing satellite lines are most likely to explain their data.

For BB Dor, one can distinguish the three components over the full orbit (compare Fig. 2) and thus answer this question: We clearly see that a crossing of the two lines occurs at phases 0.25 (red side) and 0.75 (blue side). We also point out that the phase offsets of the satellite lines are extremely symmetrical with respect to the phase of superior conjunction of the secondary. And more, if we assume that the satellite lines in the AM Her stars are also described by crossing lines, the phase offsets there show the same symmetry. Having perfect symmetry in all cases so far, seems to

indicate rather a rule than a coincidence. Therefore, assuming that the satellite lines observed in BB Dor and in the polars are stable and not just a transient feature, any explanation for the presence of these lines also has to explain their symmetry. An origin in random loops or prominences on the companion would not yield such an explanation and is thus refuted. It is rather more likely that the material in which the satellite lines are emitted is confined in two locations which are favoured by the force field of the system. Assuming that only the gravitational force is acting in the binary, this would e.g. support the idea that the material is trapped in the L4 and L5 Lagrangian points which was already discussed by Kafka et al. (2008) for AM Her. They argued against this idea because the L4 and L5 points only yield a stable equilibrium for mass ratios of $q \lesssim 0.04$ which are physically implausible for AM Her. However, one can deem similar points of equilibrium possible if the Roche geometry is modified by additional forces, e.g. the magnetic field of any of the two stars. Note that due to the general nature of the magnetic field, these equilibrium points are most likely not situated in the orbital plane of the system even though they would be bound to the orbital motion.

As a first test on the origin of the satellite lines, we computed a Doppler-tomogram of the H α emission in BB Dor using the code by Spruit (1998) with a MIDAS interface (Tappert et al. 2003). The resulting map is plotted in Fig. 3 a), the satellite lines are clearly visible as two arcs reaching out from the main triangular-shaped emission region close to the centre of mass towards positive v_y . In b)-d), we overplotted the Roche-geometry for various inclinations and mass ratios. Since the inclination of BB Dor is unknown but considered on the lower side (Chen et al. 2001) we varied it arbitrary between 30° and 60° . We used the sole dependence of a Roche-lobe-filling secondary's density with the orbital period and the mass/radius relation for low mass red dwarfs $R = M^{0.0867}$ (Hellier 2001) to derive $M_2 = 0.33 M_\odot$. With an average white dwarf mass of $M_1 = 0.8 M_\odot$ (Zorotovic et al. 2011) we calculate the mass ratio $q = 0.41$ (Fig. 3 b). The plot in Fig. 3 c) shows the results for the mass ratio $q = 0.36$ based on the revised evolutionary track by Knigge et al. (2011), while Fig. 3 d) was calculated to force a match of the two arcs with the Lagrangian points L4 and L5. For low inclinations ($30^\circ \leq i \leq 40^\circ$) and reasonable mass ratios, the L4 and L5 points fall together with the corners of the inner triangular structure. This might hint at an outflow of material through the Lagrangian points

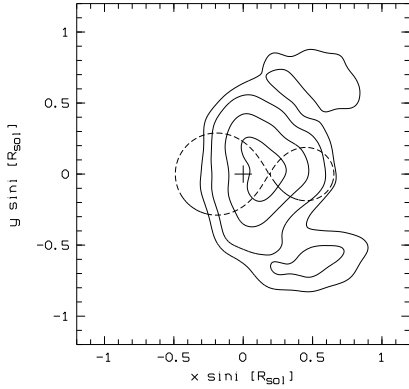


Figure 4. The H α emission distribution is plotted as solid contours in Cartesian coordinates that were calculated with the assumption that all emission sources are bound to the orbit and have no individual velocities. Overplotted in dashed lines is the Roche-geometry for $q = 0.41$ and $i = 30^\circ$.

L4 and L5. Since the agreement depends strongly on the selection of the mass ratio and the inclination, these values need to be better constrained to support such a claim.

For none of any – even generously interpreted – possible values for the mass ratio of a system just above the period gap ($0.2 < M_2/M_1 < 0.6$), a kinematic match is found between the elongated structure and the L4 and L5 points. In fact, to force such a match, a mass ratio of about 0.02 is needed which is far away from any physically reasonable value for a system with an orbital period of about 3.7 h. An explanation through pure Roche potential is thus not possible. This is in agreement with Kafka et al. (2008) who ruled out an explanation through pure Roche potential for stability reasons. Just for completeness, we note that the necessary mass ratio of $q = 0.02$ does actually yield a stable equilibrium at the L4 and L5 points as it is below the upper limit of 0.04. Again, since this critical value for the mass ratio of 0.04 is highly exceeded by systems above the period gap, they can not have a pure Roche potential with the L4 and L5 points being stable equilibrium points. One may speculate, however, whether a Roche geometry where the force field is modified by including a suitable magnetic field could actually result in the same stable equilibrium points around positions $L4_{\text{mod}}$ and $L5_{\text{mod}}$ as if the force field was purely gravitational but resulting from a low mass ratio. For binaries, such modifications of the Roche potential were performed by Dermine et al. (2009) to account for additional forces due to radiation pressure and pulsation. For single massive stars with large dipole magnetic fields, points of equilibrium between the gravitational, centrifugal and magnetic forces were modelled by Townsend & Owocki (2005) and observed by Oksala et al. (2011). It thus seems natural that similar points can also exist in close binary systems.

This could then naturally explain the distribution of the material observed here. In this picture, the presence of similar satellite lines in other close binary systems would require the right combination of gravitational and magnetic forces to yield stable equilibrium points around which the material could be confined. This might explain why these satellite lines are not observed in all systems. Since in this scenario,

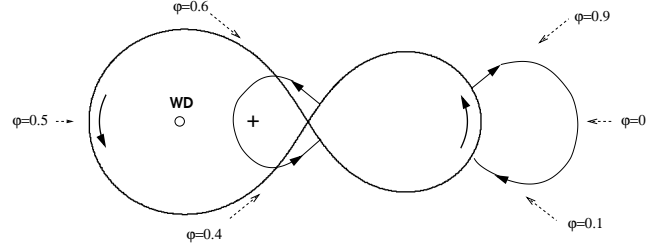


Figure 5. Sketch to illustrate the two possible orientations of prominences that could explain the observed satellite lines. Note that the scaling and in particular the size of the lobes are arbitrary.

the emission sources are co-rotating with the secondary their radial velocities can easily be converted into space coordinates using the orbital period. In Fig. 4 we have done this and for comparison overplotted the Roche lobe for $q = 0.41$ and $i = 30^\circ$.

On the other hand, the comparison with the Roche geometry only makes sense for those emission regions that are moving along with the orbit of the binary. Any velocity component vertical to the orbital plane will add to the radial velocity component within the orbital plane the radial component of this vertical velocity, which is constant over the orbital period as long as the orbit itself does not vary in space. The final result of such a vertical motion is thus a shift to the blue or red of the observed line and the effect on the Doppler map is similar to the one obtained if the system velocity is not correctly applied. However, this is not what we observe for the H α satellite lines whose zero velocity agrees with the overall system velocity as is seen in the trailed spectra diagram (Fig. 2). We can thus conclude that the satellite lines do not have a mayor vertical velocity component but their velocity vectors are confined in the orbital plane. Note that this does not imply that the material itself is actually situated in the orbital plane. It can be at any distance as long as it is moving parallel to the plane.

Since we observe the crossing of the two satellite lines, we can specifically exclude any prominences or outflows (as discussed by Kafka et al. (2008) for AM Her) that move out of the orbital plane as their origin. Any such prominence with a considerable vertical velocity component would result in shifted emission lines that move parallel to each other: their radial velocity amplitude thus belongs to the component within the orbital plane while the shift is given by the radial velocity of the vertical component. If the observed satellite lines are therefore due to prominences, these prominences have to be orientated in the following way: (1) they have to run within the orbital plane without a mayor vertical component and (2) they have to be symmetrical with respect to the axis through the white dwarf and the secondary star. To account for the maximum radial velocity being observed at phases 0.1 and 0.4, the minimum values at 0.6 and 0.9, the angle under which the material leaves the secondary must be $36 \pm 7^\circ$ on the preceding side, the angle at which it enters back must be $36 \pm 7^\circ$ on the receding side. This leaves only two possible orientations for the prominences that are illustrated in Fig. 5. We calculated the additional velocities of the prominences that would be needed to yield the observed radial velocity variation. Depending on the size of the

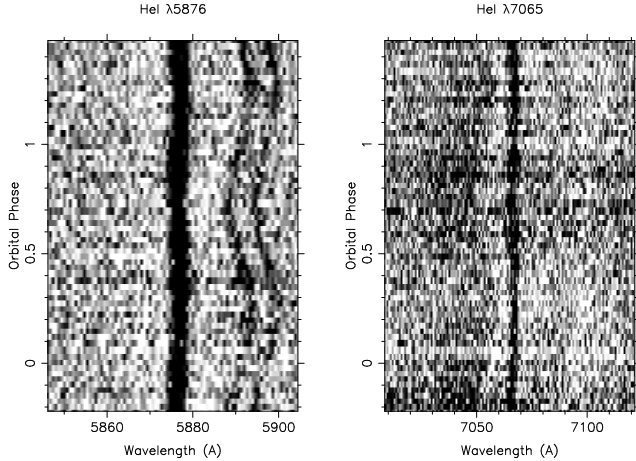


Figure 6. Left side: trailed spectra of He I λ 5876 and NaD. The difference in the amplitude of the radial velocities is clearly visible. Right side: trailed spectra of He I λ 7065. The emission line is seated inside a broad TiO absorption band that similar to NaI clearly moves with a higher velocity than the He I emission line.

secondary and the orientation of the prominence, we obtain between 200 and 350 km s⁻¹. These values are in the range of the velocities observed for coronal mass ejections from the Sun whose velocity distribution shows a strong peak around 350 km s⁻¹ (Yurchyshyn et al. 2005).

Large prominences of similar velocities are observed in fast rotating single stars like BO Mic and AB Dor. Except for the symmetry which is not present in single stars the spectral appearance is similar to what we observe in BB Dor: narrow emission lines move around the stellar disc and have radial velocity amplitudes up to ~ 550 km s⁻¹ (see e.g. Dunstone et al. 2006). For binaries, evidence for prominences comes from the X-rays. Jeffries (1996) model X-ray spectra of XY UMa and find – also in comparison with other binaries (Hall & Ramcey 1992) – that large prominences situated in the orbital plane are an apparent configuration in interacting binaries. In fact, Steeghs et al. (1996) argue that stable magnetic loops would exist in the region between L1 and the white dwarf making the presence of large slingshot prominences in this part likely.

3.3 Study of radial velocities

A detailed examination reveals that all emission lines move in phase with the secondary. In Fig. 6, the trailed spectra diagrams are plotted for the regions around He I λ 5876 and He I λ 7065. It shows the low velocity variation of the He I emission and in the left plot also the variation of the NaD doublet emission which is in phase with He and H α but displays a larger amplitude of the radial velocities. In the trailed spectra around He I λ 7065 on the right side, a broad TiO absorption trough mimics the motion of the NaD lines but has an even larger velocity amplitude.

Quantitatively, these results are supported by the phase folded radial velocity curves plotted in Fig. 7. For the He I λ 5878, He I λ 6678, and He I λ 7065 emission lines, the radial velocities were measured by fitting single Gaussians of 300 km s⁻¹ width to the lines. All three lines follow the same variation. However, He I λ 7065 is very noisy, the line is not

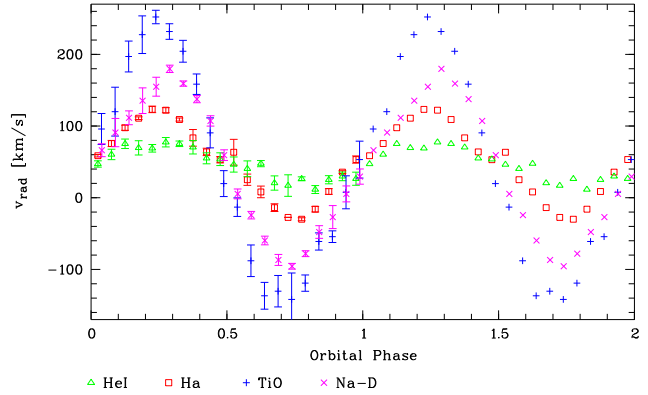


Figure 7. Phase-binned radial velocities are plotted for the H α , He I, and NaD emission lines and for a TiO absorption trough.

Table 1. The parameters of the sine fit $\gamma + k \cdot \sin 2\pi(\phi - \phi_0)$ to the radial velocities

	ϕ_0	γ [km s ⁻¹]	k [km s ⁻¹]
He I	0.023(07)	46.8(9)	28.5(12)
H α	-0.010(03)	48.8(8)	67.8(11)
NaD	-0.013(03)	41(2)	124(2)
TiO	-0.040(03)	na	186(3)

always detected in the single spectra so we decided to only use He I λ 5878 and He I λ 6678 and averaged them within each phase bin. The NaD emission lines and the TiO absorption bands were generally too weak to be measured in the individual spectra. Instead, we averaged data from the same orbital phase without changing the time-resolution and plotted them as trailed spectra. For TiO, we manually followed the position of the edge of the absorption trough at 7052 Å on these trailed spectra. We independently determined its radial velocities three times. For NaD, we manually measured the radial velocities of each line twice. This gave four independent measurements which were then phase binned. For all methods, the error is determined as the sigma of the distribution of the radial velocities within the bin size of 0.05 phases. To confirm the manual measurement of the radial velocities by a more robust technique, we subtracted velocity sine waves with amplitudes ranging from 115 to 125 km s⁻¹ to the 65 spectra to eliminate the motion of the NaD lines. Radial velocity curves of the almost-straight NaI lines were constructed and their deviation from the mean measured. We then fitted a parabola to the velocity amplitude-sigma data and measured its minimum as the correct velocity amplitude $K_2 = 118 \pm 4$ km s⁻¹. This value is in agreement with the one found by the manual method described above (see Table 1).

Monte Carlo sine fits to the data (for the resulting parameters, see Table 1) show that the phase shifts of all radial velocity curves are in agreement with the average value indicating that all analysed lines have their origin on the side of the secondary star. The system velocity γ is determined as 48 ± 2 km s⁻¹. As easily seen in Fig. 7, the amplitude of the radial velocity varies, however, significantly for different lines; the exact values are given in Table 1. It is to note that for H α our value $k = 67.8 \pm 1.1$ km s⁻¹ differs signifi-

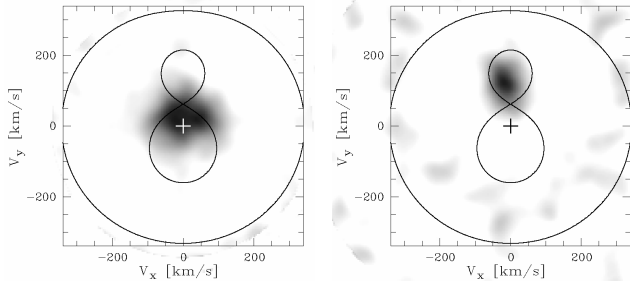


Figure 8. Doppler maps of He I (left) and Na D (right), see text for details. Overplotted is the Roche geometry for $M_2/M_1 = 0.41$ and $i = 30^\circ$. For comparison, the plot of H α with the same Roche geometry is in Fig. 3 b).

cantly from the one derived by Rodríguez-Gil et al. (2012) $k = 99 \pm 2 \text{ km s}^{-1}$. This is probably due to the lower spectral resolution of Rodríguez-Gil et al. (2012) such that they do not resolve the satellite lines which will then contribute to the overall radial velocity. As a test, we smeared our spectra with a Gaussian of 5.4 \AA and measured the radial velocities of H α with a Gaussian of 400 km s^{-1} thus including the satellite lines and simulating the data and measurements of Rodríguez-Gil et al. (2012). From these we obtain a value $k = 79 \pm 1 \text{ km s}^{-1}$ which is in slightly better agreement with Rodríguez-Gil et al. (2012) and thus confirms that their radial velocity amplitude is at least partly increased due to the unresolved component of the satellite lines.

The different velocity amplitude for the various narrow emission lines can be explained by assuming a temperature gradient on the secondary star as is expected for an irradiated object. He I, which needs the highest temperature to be excited is only present where the secondary star is closest to the white dwarf, i.e. around L1. The temperature to excite hydrogen to emit H α is lower, hence the irradiated region on the secondary which emits H α is larger and due to the bound rotation of the secondary reaches to higher velocities. The Na lines instead are probably chromospheric and thus trace the motion of the secondary's centre of mass, while the TiO absorption bands come from the non-irradiated backside of the secondary.

For the He and Na emission lines, this behaviour is visualised in Fig. 8. Here, we computed the Doppler maps for He I $\lambda 5878$, He I $\lambda 6678$, and He I $\lambda 7065$ individually and averaged them to increase the S/N ratio. For the Na doublet instead, the two lines were too close for computing individual Doppler maps. Instead, we shifted each spectrum by 5.97 \AA – the wavelength difference between the two lines – and averaged it with the non-shifted spectrum. This yields a central averaged line and two outer lines of half the strength which appear in the Doppler map as an artificial structure following an outer ring centred around the Na emission source which has to be ignored. It is clear from the Doppler maps in Fig. 3 and 8 that the regions of line emission are different for each element and qualitatively follow the expected temperature distribution for an irradiated secondary star if a mass ratio of $q \geq 0.4$ is assumed. For smaller mass ratios, the Roche-geometry changes such that the irradiated material would originate rather in the area between L1 and the centre of rotation.

4 CONCLUSIONS

We observed BB Dor during a low state using medium resolution VLT/FORS2 spectroscopy around H α . By comparing the line profiles and the continuum with the results of Rodríguez-Gil et al. (2012) we can conclude that no detectable accretion happened during this observing run.

We detect H α , He I, and Na I emission lines as well as TiO absorption bands which trace the motion of different temperature zones of the irradiated secondary star. Given that He I and H α originate at the higher temperature regions of the secondary close to L1 (which is reflected in their low velocity amplitude) and TiO bands are likely to originate in the non-irradiated, cooler, backside zones of the secondary star, we judge that the velocity measured from the Na I lines which are likely of chromospheric origin reflects best the projected velocity of the secondary. We thus determine the radial velocity amplitude $K_2 = 118 \pm 4 \text{ km s}^{-1}$ for the secondary star.

In H α , we find satellite lines similar to those seen in AM Her in quiescence. Our data show clearly that these are described by two crossing sinusoidal curves with the same radial velocity amplitude of 340 km s^{-1} , larger than that of the central line or even than K_2 . As in the case of AM Her, they are symmetrically offset by ± 0.15 phases.

If the H α satellites were emitted by material trapped in the L4 and L5 Lagrangian points, following the standard Roche model the necessary mass ratio would be 0.02. Even though this value would actually yield stable equilibria, it does not agree with the possible masses for the components of a CV with an orbital period of nearly four hours. The interpretation of trapping the material by a pure Roche potential is thus refuted. Additional forces, probably of magnetic nature, are needed to modify the Roche potential to keep the observed H α -emitting material in a stable configuration. We point out that the white dwarf in BB Dor is not strongly magnetic. With less than 5 MG, its strength is not comparable to AM Her. Still, the observed satellite lines are strikingly similar. We thus conclude that they are not likely caused by the magnetic field of the white dwarf as was suggested for the case of AM Her (Kafka et al. 2008). We rather favour the influence of the magnetic field of the secondary as an explanation for the two additional emission sources. A modified Roche geometry taking into account such an additional force might result in stable equilibrium points around the positions where the increased emission is observed.

The other way of explaining the presence of the satellite lines would be for H α -emitting material moving in prominences originating in a magnetically active secondary star. To explain the observed variation of the satellite lines, only two orientations are possible for these prominences. In this picture the similarities between the satellite lines in different CVs are either coincidental or more likely are caused by a preferential orientation of prominences in a fast orbiting binary star.

ACKNOWLEDGEMENTS

Partially funded by the Spanish MICINN under the Consolider-Ingenio 2010 Program grants CSD2006-00070: First Science with the GTC and CSD2009-00038: ASTRO-

MOL. PRG thanks ESO for a stay within the Visitor Scientist program. The use of MOLLY developed by Tom Marsh is gratefully acknowledged. We thank the team on Paranal for taking the spectra in ToO mode, i.e. Emanuela Pompei and Thomas Rivinius.

REFERENCES

- Appenzeller I., Fricke K., Fürtig W., Gässler W., Häfner R., Harke R., Hess H.-J., Hummel W., Jürgens P., Kudritzki R.-P., Mantel K.-H., Meisl W., Muschiolok B., Nicklas H., Rupprecht G., et al. 1998, *Messenger*, 94, 1
- Araujo-Betancor S., Knigge C., Long K. S., Hoard D. W., Szkody P., Rodgers B., Krisciunas K., Dhillon V. S., Hynes R. I., Patterson J., Kemp J., 2003, *ApJ*, 583, 437
- Chen A., O'Donoghue D., Stobie R. S., Kilkenny D., Warner B., 2001, *MNRAS*, 325, 89
- Dermine T., Jorissen A., Siess L., Frankowski A., 2009, *A&A*, 507, 891
- Dunstone N. J., Collier Cameron A., Barnes J. R., Jardine M., 2006, *MNRAS*, 373, 1308
- Gänsicke B. T., Sion E. M., Beuermann K., Fabian D., Cheng F. H., Krautter J., 1999, *A&A*, 347, 178
- Godon P., Sion E. M., Barrett P. E., Szkody P., Schlegel E. M., 2008, *ApJ*, 687, 532
- Hall J. C., Ramcey L. W., 1992, *AJ*, 104, 1942
- Hellier C., 2001, *Cataclysmic Variable Stars*. Springer
- Hoard D. W., Linnell A. P., Szkody P., Fried R. E., Sion E. M., Hubeny I., Wolfe M. A., 2004, *ApJ*, 604, 346
- Horne K., 1986, *PASP*, 98, 609
- Jeffries R. D., 1996, in K. G. Strassmeier & J. L. Linsky ed., *Stellar Surface Structure Vol. 176 of IAU Symposium*, p. 461
- Kafka S., Honeycutt R. K., Howell S. B., 2006, *AJ*, 131, 2673
- Kafka S., Honeycutt R. K., Howell S. B., Harrison T. E., 2005, *AJ*, 130, 2852
- Kafka S., Howell S. B., Honeycutt R. K., Robertson J. W., 2007, *AJ*, 133, 1645
- Kafka S., Ribeiro T., Baptista R., Honeycutt R. K., Robertson J. W., 2008, *ApJ*, 688, 1302
- Kafka S., Tappert C., Ribeiro T., Honeycutt R. K., Hoard D. W., Saar S., 2010, *ApJ*, 721, 1714
- Knigge C., Araujo-Betancor S., Gänsicke B. T., Long K. S., Szkody P., Hoard D. W., Hynes R. I., Dhillon, V. S. 2004, *ApJ*, 615, L129
- Knigge C., Baraffe I., Patterson J., 2011, *ApJS*, 194, 28
- Latham D. W., Liebert J., Steiner J. E., 1981, *ApJ*, 246, 919
- Mason E., Howell S. B., Barman T., Szkody P., Wickramasinghe D., 2008, *A&A*, 490, 279
- Oksala M. E., Wade G. A., Townsend R. H. D., Owocki S. P., Kochukhov O., Neiner C., Alecian E., Grunhut J., 2011, *MNRAS*, p. 1620
- Rodríguez-Gil P., Gänsicke B. T., Hagen H.-J., Araujo-Betancor S., Aungwerojwit A., et al. 2007, *MNRAS*, 377, 1747
- Rodríguez-Gil P., Schmidtbreick L., Long K. S., Gänsicke B. T., Torres M. A. P., Rubio-Díez M. M., Santander-García M., 2012, *MNRAS*, submitted
- Rodríguez-Gil P., Schmidtbreick L., Gänsicke B. T., 2007, *MNRAS*, 374, 1359
- Rodríguez-Gil P., Schmidtbreick L., Long K. S., Shahbaz T., Gänsicke B. T., Torres M. A. P., 2011, *ArXiv e-prints*
- Schwarzenberg-Czerny A., 1989, *MNRAS*, 241, 153
- Shafter A. W., Szkody P., Liebert J., Penning W. R., Bond H. E., Grauer A. D., 1985, *ApJ*, 290, 707
- Spruit H. C., 1998, *ArXiv Astrophysics e-prints*
- Steeeghs D., Horne K., Marsh T. R., Donati J. F., 1996, *MNRAS*, 281, 626
- Tappert C., Mennickent R. E., Arenas J., Matsumoto K., Hanuschik R. W., 2003, *A&A*, 408, 651
- Thorstensen J. R., Ringwald F. A., Wade R. A., Schmidt G. D., Norsworthy J. E., 1991, *AJ*, 102, 272
- Townsend R. H. D., Owocki S. P., 2005, *MNRAS*, 357, 251
- Townsend R. H. D., Gänsicke B. T., 2009, *ApJ*, 693, 1007
- Young A., Rottler L., Skumanich A., 1991, *ApJ*, 378, L25
- Yurchyshyn V., Yashiro S., Abramenko V., Wang H., Gopalswamy N., 2005, *ApJ*, 619, 599
- Zorotovic M., Schreiber M. R., Gänsicke B. T., 2011, *A&A*, 536, A42

This paper has been typeset from a \LaTeX file prepared by the author.